Formation Mechanism of Oxide Scales Grown on X10CrAlSi18 and 310S Heat-Resistant Stainless Steels Under High Temperature in Air

Yuqing Zhou, Dening Zou, Wei Zhang, Yingbo Zhang and Lei Du

Abstract To promote the application of resource-saving heat-resistant stainless steels, the study on high temperature oxidation behavior and oxide-scales formation mechanism of X10CrAlSi18 ferritic heat-resistant stainless steels (FHSSs) and 310S austenitic heat-resistant stainless steels (AHSSs) was carried out in air up to 140 h, and the microstructure of oxide scales, oxidation kinetics and thermodynamics theories, and the classical hypothesis of the third-element effect analyzed. The results showed that the cost-effective X10CrAlSi18 FHSSs presented good oxidation resistance at 800 and 900 °C due to the compact multicomponent oxide scales composed of Al_2O_3, Cr_2O_3, $MnCr_2O_4$ and $MnFe_2O_4$ and good adhesion to the matrix. However, the oxidation resistance of the alloy at 1000 °C was deteriorated, which is mainly due to the non-protective Fe_2O_3. The oxide scales of 310S AHSSs containing Cr_2O_3, $MnCr_2O_4$ and inner SiO_2 exhibited good oxidation resistance, while the internal oxidation of silicon weakened the adhesion to the substrate.

Keywords Heat-resistant stainless steel · Austenite and ferrite · Third-element effect · Oxidation mechanism

Y. Zhou · D. Zou (✉) · Y. Zhang · L. Du
School of Metallurgy and Engineering, Xi'an University of Architecture and Technology, Xi'an 710055, China
e-mail: zoudening@sina.com

Y. Zhou
e-mail: zhouyuqing324@163.com

Y. Zhang
e-mail: 347135652@qq.com

L. Du
e-mail: 794345727@qq.com

W. Zhang
State Key Laboratory for Mechanical Behavior of Materials, Xi'an Jiaotong University, Xi'an 710049, China
e-mail: 4097567@qq.com

© Springer Nature Singapore Pte Ltd. 2018

Y. Han (ed.), *High Performance Structural Materials*,
https://doi.org/10.1007/978-981-13-0104-9_81

Introduction

AHSSs have been widely used in power plants [1] due to good oxidation and creep resistance and comprehensive mechanical properties. However, the tight supply and expensive price of nickel resource make AHSSs uneconomical [2], so cost-effective FHSSs have gradually replaced AHSSs in some applications of high temperature fields due to high thermal conductivity, low linear expansion coefficient and good mechanical strength and formability [3–5]. Nowadays, 310S AHSSs as the main boiler-pipeline alloys have been widely used in power plants [6], and previous studies [7–9] show that FHSSs which contain Al and Si synergizing with Cr may exhibit extremely good oxidation resistance, so we attempt to substitute 310S AHSSs by nickel-free X10CrAlSi18 FHSSs with lower Cr content and some Al and Si elements.

High temperature oxidation resistance of heat-resistant steels is one of the principal properties applied in power generation, and the key to obtain good resistance is to establish an external, continuous layer of slow-growing and thermodynamically stable oxide scales. Much work has been done on oxidation resistance of AHSSs, but the oxide-scales formation mechanism of 310S AHSSs is not explicit enough and the oxidation behavior of X10CrAlSi18 FHSSs is not reported before, so we comparatively investigated the high temperature oxidation behavior and oxide-scales formation mechanism of X10CrAlSi18 FHSSs and 310S AHSSs to promote the substitution of 310S AHSSs by nickel-free X10CrAlSi18 FHSSs.

Materials and Methods

Chemical compositions of X10CrAlSi18 FHSSs and 310S AHSSs are shown in Table 1. The specimens were cut from hot-rolling plates with dimensions of 30 mm × 15 mm × 4 mm. The surfaces of specimens were grounded with SiC water-abrasive papers up to No. 2000 to remove the surface oxide skin, and then cleaned by ethanol and dried in the oven. The total weight of "specimen + crucible" both before and after oxidation tests was weighted by microbalance with a resolution of 10^{-4} g to obtain the mass gain.

The isothermal oxidation test was carried out in air by box-type electric-resistance heating furnace, due to the difference of working temperature between FHSSs and AHSSs, the oxidation temperature of X10CrAlSi18 FHSSs is

Table 1 Chemical compositions of X10CrAlSi18 FHSSs and 310S AHSSs [wt%]

Steel	C	Si	Mn	P	S	Cr	Al	Ni
X10CrAlSi18	0.085	1.04	0.93	0.008	0.006	17.91	1.03	0
310S	0.07	0.75	1.8	0.03	0.001	25	0	19

800, 900 and 1000 °C, while that of 310S AHSSs is 800, 900, 1000 and 1100 °C. And the oxidation time both is 20, 40, 60, 80, 100, 120 and 140 h. After the oxidation test, the variations of mass gain were evaluated to determine the oxidation kinetics. The cross-section morphologies and chemical compositions of oxide scales were investigated by scanning electron microscope (SEM) equipped with electron dispersive spectroscopy (EDS). The phase constitutions of oxide scales were detected by X-ray diffractometer (XRD). Then the high temperature oxidation behavior and oxide-scales formation mechanism were researched based on the oxidation kinetics and thermodynamics theories and the classical hypothesis of the third-element effect.

Results and Discussion

Kinetics and Thermodynamics Theories and the Hypothesis Wagner theory [10, 11] confirms that kinetic curves of oxidation resistance materials obey the parabolic regime, which is at the initial oxidation stage, the chemical adsorption and reaction decide the oxide scale formation, and the diffusion of solutes through the substrate to scale-metal interface mainly by grain-boundary diffusion is important in determining the compositions of oxide scales under this situation [12]. Then at the oxide scale growth stage, oxidation is controlled by the migration of solutes across oxide scales by grain boundaries and vacancies. It can be deduced that the slightly increased mass gain in this stage is attributed to the lower diffusion coefficients [13] in compact oxide scales.

The Richardson-Ellingham diagram of thermodynamics theory [14] revealing the relationship between standard Gibbs-free energy and oxidation temperature indicates the probability and order of chemical oxidation reactions. This exhibits the affinity between oxygen and other elements and the possible order of oxidation products. However, the final oxidation behavior also combines with the content of alloy elements and oxidation kinetics.

The classical hypothesis of the third-element effect [15–18] is that an element with an oxygen affinity between the basis metal and protective oxide-forming element can promote the establishment of the protective scale by acting as a secondary getter for oxygen, thereby decreasing the inward flux of oxygen into the substrate when the primary getter is removed from the surface regions as its oxide. Meanwhile, the third-element effect also prevents the formation of non-protective scale by suppressing the outward flux of base metal, such as iron.

Oxidation Mechanism of X10CrAlSi18 FHSSs Figure 1a shows the isothermal oxidation kinetic curves of X10CrAlSi18 FHSSs at different temperatures. This indicates that the mass gain per unit at 1000 °C is apparently higher than that at 800 and 900 °C, and the weight gain curves present a parabolic law of Wagner theory [10, 11]. XRD analysis of oxide scales of X10CrAlSi18 FHSSs at different temperatures for 140 h is shown in Fig. 1b. It should be noted that the oxidation

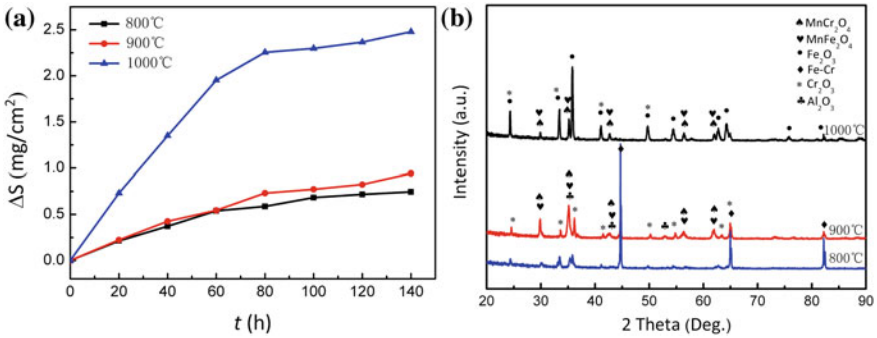

Fig. 1 **a** Isothermal oxidation kinetic curves of X10CrAlSi18 FHSSs at different temperatures in air; **b** XRD analysis of oxide scales of X10CrAlSi18 FHSSs at different temperatures for 140 h in air

products of X10CrAlSi18 FHSSs are vary with different oxidation temperatures. The products are Cr_2O_3, Al_2O_3, $MnFe_2O_4$ and $MnCr_2O_4$ at 800 and 900°C and turn into Fe_2O_3, Cr_2O_3, $MnFe_2O_4$ and $MnCr_2O_4$ at 1000 °C.

The cross-section EDS analysis of the oxide scales at 800 and 1000 °C for 140 h is shown in Fig. 2. It can be observed from Fig. 2a that Al, Mn, Si and Cr elements almost simultaneously diffuse to external, and the content of Al_2O_3 in inter part is relatively high, the content of Cr_2O_3 in middle part is slightly high, and Al_2O_3, spinel $MnFe_2O_4$ and $MnCr_2O_4$ almost assemble in the outer part. This is a homogenous, compact, continuous and well-adherent multicomponent oxide scale. It should be noted from Fig. 2b that the oxide scale exhibits delamination and the situation is complicated at 1000 °C, and chromium continuously distributes in the outer layer and there is a discontinuous distribution of iron in its interior. In addition, silicon and lots of aluminum exist in the inner layer. As for manganese and oxygen, they exist in the whole layer of the oxide scale, and manganese mainly gathers in the outermost and the innermost layers. This indicates that oxide scale of 1000 °C is divided into three layers, the inner layer distributes Al_2O_3 and SiO, the middle layer exists Cr_2O_3 and Fe_2O_3, and the outer layer is composed of spinel $MnFe_2O_4$ and $MnCr_2O_4$.

Based on the Richardson-Ellingham diagram, the possible order of oxidation products of X10CrAlSi18 FHSSs is: $Al_2O_3 > SiO_2 > MnO > Cr_2O_3 > Fe_3O_4 > Fe_2O_3$ [14]. Combined with the theories and the analysis of microstructure of oxide scales, the formation mechanism of oxide scales of X10CrAlSi18 FHSSs can be summarized as:

When the oxidation temperature is 800 and 900 °C, at the initial oxide formation stage, aluminum and silicon have high affinity for oxygen among other elements, so they primarily precipitate from the alloy matrix, however, silicon is much less effective than aluminum in rapidly developing a oxide layer [15], so massive Al_2O_3 is detected while SiO_2 was not detected at 800 °C. It should be noted form the hypothesis of the third-element effect that chromium as for the third-element in

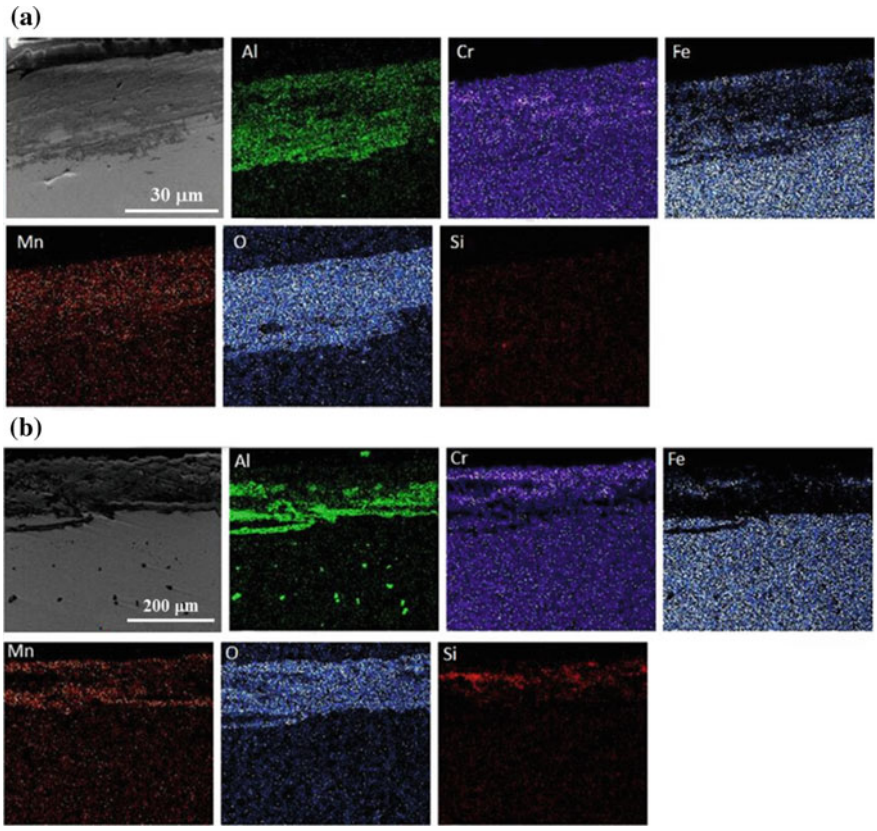

Fig. 2 Cross-section EDS of oxide scales of X10CrAlSi18 FHSSs for 140 h in air: **a** at 800 °C; **b** at 1000 °C

X10CrAlSi18 FHSSs facilitates the establishment of Al_2O_3 and prohibits aluminum precipitating out as internal oxides embedded into the substrate, meanwhile, chromium with high content also generates massive Cr_2O_3. Related research [19] shows that with Al_2O_3 oxide scales have low growth rates and good thermodynamically stability compared with those of Cr_2O_3 scales. Then at the scale-growth stage, the vacancies and grain boundaries of oxide scale offer short-circuit diffusion path for outward diffusion of Fe^{3+} and Mn^{2+} and inward diffusion of O^{2-} [20]. The spinel oxides are more stable than binary oxides, so Fe^{3+} and Mn^{2+} migrating to external react with oxygen to form MnO and Fe_2O_3, then binary Fe_2O_3 and Cr_2O_3 react with MnO to form spinel $MnFe_2O_4$ and $MnCr_2O_4$ immediately.

When the oxidation temperature is 1000 °C, the third-element effect is reduced due to the higher temperature, so oxygen solubility and diffusivity in the substrate largely increase and solutes (such as Al and Cr elements) rapidly deplete at the initial oxide formation stage. Therefore, that gives a chance for iron to react with

oxygen to form non-protective Fe_2O_3 and the oxide scale is apparently thicker than that of 800 and 900 °C. This results the oxidation resistance at 1000 °C is deteriorated.

Oxidation Mechanism of 310S AHSSs The isothermal oxidation kinetic curves of 310S AHSSs at different temperatures are shown in Fig. 3a, which illustrates that the mass gain per unit at 1100 °C is remarkably higher than that at 800, 900 and 1000 °C, and the mass gain curves almost present parabolic regime of Wagner theory [13, 14]. Figure 3b presents the phase constitutions of oxide scales at different temperatures for 140 h. It is found that the oxide scales of 310S AHSSs is composed of Cr_2O_3, spinal [21] $MnCr_2O_4$ and substrate FeCr(Ni) at 800 °C, while the substrate FeCr(Ni) is not detected at 900, 1000 and 1100 °C. This reveals that the oxidation products of 310S AHSSs are same with different oxidation temperature, only the oxide scale is thicken with the higher oxidation temperature.

The cross-section EDS analysis of the oxide scale at 900 and 1100 °C for 120 h is shown in Fig. 4. It is concluded from Fig. 4a that a continuous and dense external Cr_2O_3 and $MnCr_2O_4$ oxide scale formed, and silicon assembles in the scale-metal interface and embeds into the substrate, so there exists internal oxidation of silicon and the scale is not well adherent to the substrate. Figure 4b shows that the higher the oxidation temperature is, the thicker and rougher the external oxide scale becomes and the severer the internal oxidation of silicon becomes.

Based on the Richardson-Ellingham diagram, the possible order of oxidation products of 310S AHSSs is: $SiO_2 > MnO > Cr_2O_3 > FeO > Fe_3O_4 > NiO > Fe_2O_3$ [14]. Combined with the theories and the analysis of microstructure of oxide scales, the formation mechanism of oxide scales grown on 310S AHSSs can be summarized as:

At the initial oxide formation stage, SiO_2 primarily forms in the internal oxide scale due to its highest affinity with oxygen, and it should be noted form the third-element effect hypothesis that chromium as for the third-element in 310S AHSSs will promote the formation of SiO_2, however, the silicon content is low and

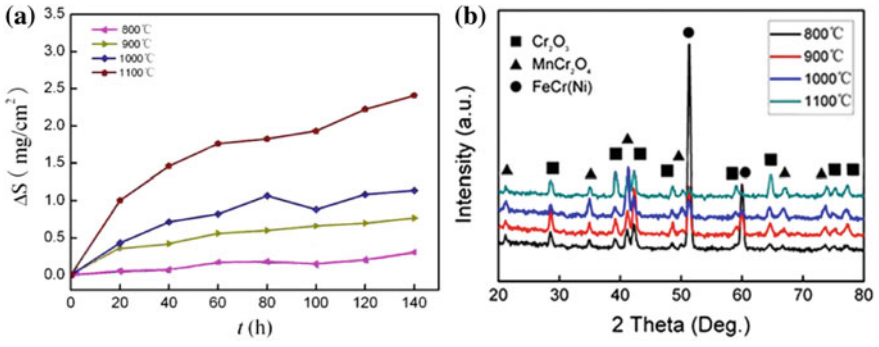

Fig. 3 **a** Isothermal oxidation kinetic curves of 310S AHSSs at different temperatures in air; **b** XRD analysis of the oxide scales of 310S AHSSs at different temperatures for 140 h in air

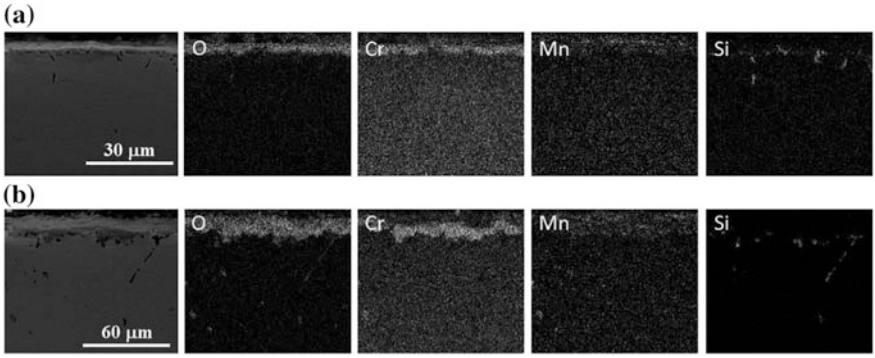

Fig. 4 Cross-section EDS of oxide scales of 310S AHSSs for 120 h in air: **a** at 900 °C; **b** at 1100 °C

silicon is not effective enough in rapidly developing a healing layer of its oxide [15], so the effect of the third-element is reduced, and SiO_2 forms slowly and exhibits pronounced protrusions into the substrate. Meanwhile, massive Cr_2O_3 formed in the interface due to its high content. Then at the scale-growth stage, the vacancies and grain boundaries of Cr_2O_3 scale offer the short-circuit diffusion path for outward diffusion of Mn^{2+} and inward diffusion of O^{2-} [20]. It is known that the standard Gibbs-free energy of the formation for the spinel oxides is more negative than the binary oxides. Therefore, when Mn^{2+} migrates to the outward of scale, it reacts with oxygen to form MnO, then Cr_2O_3 reacts with MnO to form spinel $MnCr_2O_4$ immediately and a diffusion barrier against high temperature oxidation constitutes.

Conclusion

Nickel-free X10CrAlSi18 FHSSs with lower Cr content and additional Al and Si elements exhibit good oxidation resistance at 800 and 900 °C due to dense, continuous and homogenous multicomponent oxide scales containing Al_2O_3, Cr_2O_3, $MnFe_2O_4$ and $MnCr_2O_4$ and well adherent to the matrix, while the oxidation resistance is deteriorates at 1000 °C mainly because of the formation of non-protective Fe_2O_3 scales. Oxide scales of 310S AHSSs are composed of continuous and dense Cr_2O_3 and $MnCr_2O_4$, but silicon exhibits severe internal oxidation embedded into the substrate. Therefore, the adherence between oxide scales and substrate and oxidation resistance were relatively deteriorated. X10CrAlSi18 FHSSs can substitute 310S AHSSs applying in the power plants when the oxidation temperature is not higher than 900 °C.

Acknowledgements The authors acknowledge the support of this work by the Iron and Steel Joint Fund of National Natural Science Foundation of China (U1460104), National Natural Science Foundation of China (51774226), and Scientific Research Program of Shaanxi Education Department (17JF013).

References

1. N. Karimi, F. Riffard, F. Rabaste, S. Perrier, R. Cueff, C. Issartel, H. Buscail, Characterization of the oxides formed at 1000 °C on the AISI 304 stainless steel by X-ray diffraction and infrared spectroscopy, J. App. Surf. Sci. 254 (2008) 2292–2299.
2. H. Yan, H. Bi, X. Li, Z. Xu, Mater. Charact. 60 (2009) 65–68.
3. E.H. Saarivirta, V.T. Kuokkala, P. Pohjanne, Thermally grown oxide films and corrosion performance of ferritic stainless steels under simulated exhaust gas condensate conditions, Corros. Sci. 87 (2014) 344–365.
4. Y. Xu, X. Zhang, L. Fan, Improved oxidation resistance of 15 wt.% Cr ferritic stainless steels containing 0.08–2.45 wt.% Al at 1000 °C in air, Corros. Sci. 100 (2015) 311–321.
5. L. Xin, S. Jun, B.H. yun, High-temperature oxidation behavior of ferritic stainless steel containing molybdenum, J. Iron and Steel Res. 5 (2013) 54–58.
6. L.P. Qing, Z. Peng, L. Hui, M. Qian, W. Y. Peng, Effect of solution treatment on microstructure and properties of high-alumina 310S steel, T. Mater. Heat Treat. 35 (2014) 73–78.
7. H. Fujikawa, S.B. Newcomb, High temperature oxidation behavior of high Al content ferritic and austenitic stainless steels with and without rare-earth element addition, Oxid. Met. 77 (2012) 85–92.
8. T. Liu, C. Wang, H. Shen, W. Chou, N.Y. Iwata, A. Kimura, The effects of Cr and Al concentrations on the oxidation behavior of oxide dispersion strengthened ferritic alloys, Corros. Sci. 76 (2013) 310–316.
9. T.J. Park, J.P. Kong, S.H. Uhm, I.S. Woo, J.S. Lee, C.Y. Kan, Effect of Al–Si coating layer on the penetration and microstructures of ferritic stainless steel, 409L GTA welds, J. Mater. Proc. Tech. 211 (2011) 415–423.
10. D.J. Young, High temperature oxidation and corrosion of metals, Elsevier, London, 2008.
11. C. Wagner, Theoretical analysis of the diffusion processes determining the oxidation rate of alloys, J. Electro. chem. Soc. 99 (1952) 369–80.
12. J.G. Goedjen, D.A. Shores, The effect of alloy grain size on the transient oxidation behavior of an alumina-forming alloy, Oxid. Metals. 37 (1992) 125–42.
13. R. Haugsrud, On the high-temperature oxidation of nickel, Corros.Sci. 45 (2003) 211–35.
14. L.M. shuan, High-temperature corrosion of materials, Press Metall. Industry, Beijing, 2002.
15. F.H. Stott, G. C. Wood, J. Stringert, The influence of alloying elements on the development and maintenance of protective scales, Oxid. Metals. 44 (1995) 113–45.
16. C. Wagner, Corros. Sci., 5, 751 (1965).
17. M.G. Hobby, M.Sc. Thesis, Univ. of Manchester (1968).
18. W.C. Hagel, Corrosion, 21, 316 (1965).
19. L.F. He, P. Roman, B. Leng, K. Sridharan, M. Anderson, T.R. Allen, Corrosion behavior of an alumina forming austenitic steel exposed to supercritical carbon dioxide, Corros. Sci. 82 (2014) 67–76.
20. G. Fu, L. Wei, Influence of a Cr_2O_3 glass coating on enhancing the oxidation resistance of 20MnSiNb structural steel, Sur. and Coatings Tech. 294 (2016) 8–14.
21. D.S. Li, Q.X. Dai, et al, High-temperature oxidation resistance of austenitic stainless steel Cr18Ni11Cu3Al3MnNb, J. Iron and Steel Res. Int. 19 (2012) 74–78.